

# Large-scale design of robust genetic circuits with multiple inputs and outputs for mammalian cells

Benjamin H Weinberg<sup>1</sup>, N T Hang Pham<sup>1</sup>, Leidy D Caraballo<sup>1</sup>, Thomas Lozanoski<sup>1</sup>, Adrien Engel<sup>1,2</sup>, Swapnil Bhatia<sup>3</sup> & Wilson W Wong<sup>1</sup>

Engineered genetic circuits for mammalian cells often require extensive fine-tuning to perform as intended. We present a robust, general, scalable system, called ‘Boolean logic and arithmetic through DNA excision’ (BLADE), to engineer genetic circuits with multiple inputs and outputs in mammalian cells with minimal optimization. The reliability of BLADE arises from its reliance on recombinases under the control of a single promoter, which integrates circuit signals on a single transcriptional layer. We used BLADE to build 113 circuits in human embryonic kidney and Jurkat T cells and devised a quantitative, vector-proximity metric to evaluate their performance. Of 113 circuits analyzed, 109 functioned (96.5%) as intended without optimization. The circuits, which are available through Addgene, include a 3-input, two-output full adder; a 6-input, one-output Boolean logic look-up table; circuits with small-molecule-inducible control; and circuits that incorporate CRISPR–Cas9 to regulate endogenous genes. BLADE enables execution of sophisticated cellular computation in mammalian cells, with applications in cell and tissue engineering.

A fundamental goal of synthetic biology is to predictably and efficiently reprogram cells to perform computations and carry out specific biological tasks<sup>1</sup>. Cells genetically engineered with biocomputation circuits hold great promise for improving therapeutics<sup>2–5</sup>, diagnostics<sup>6,7</sup>, animal models<sup>8,9</sup>, and industrial biotechnological processes<sup>10,11</sup>. Despite rapid advances and promising results in biocomputation design<sup>12–16</sup>, implementing simple 2-input, single-output Boolean functions in prokaryotic and eukaryotic cells necessitates the layering of multiple genetic circuits, requiring extensive construction and tuning of genetic components. Circuits with multiple inputs and multiple outputs remain scarce in the scientific literature owing to the need of a large library of interoperable genetic parts and the compounding effects of connecting increasingly more transcriptional components together into single cells<sup>17</sup>. Curation of genetic circuit components and the development of automated design software are starting to address these problems in bacteria<sup>18–22</sup>, but are not currently available for mammalian cells. It is not clear whether either parts or design software can be transferred from bacteria to higher organisms.

To facilitate the construction of genetic circuits in eukaryotic cells, we present BLADE, a general framework for engineering complex logic circuits in mammalian cells using site-specific recombinases. In contrast to previous approaches for circuit design, BLADE requires minimal optimization by the user and readily yields circuits with multiple inputs or outputs without increasing the number of transcription units.

We use our system to design, build, and test >100 functionally distinct circuits, including some of the most complex logical operations engineered in any living cell to date. BLADE accommodates

multiple outputs without adding to design complexity and can be adapted to regulate the expression of mRNAs from Pol II promoters, or non-coding regulatory RNAs from Pol III promoters, such as CRISPR–Cas9 guide RNAs. Being able to build complex logic circuits that control multiple different guide RNAs could enable exquisite control of endogenous mammalian gene expression.

## RESULTS

### Characterization of recombinases

Site-specific DNA recombinases, which are a class of DNA-modifying enzymes that recognize a specific DNA sequence and perform cleavage and reunion of DNA<sup>23</sup>, show promise for use in building synthetic circuits in eukaryotic cells. This is due in part to their versatility to simultaneously function as transcriptional activators and repressors within the same cell on the same transcription unit; a feat that is difficult to achieve with transcription factors. Recombinase-mediated gene expression can be achieved by tyrosine-recombinase-mediated excision of a transcription terminator located upstream of a gene of interest (GOI) or serine-integrase-mediated inversion of a GOI (analogous to a buffer ‘BUF’ gate) (Fig. 1a). Conversely, termination of gene expression can be achieved by the placement of recombination sites around a GOI and elimination of gene expression using tyrosine-recombinase-mediated excision or serine integrase inversion (analogous to a NOT gate).

Multi-input recombinase-based biological computational circuits require robust and orthogonal genetic components. Here, 12 recombinases, including both tyrosine recombinase and serine integrase families were tested for activity and orthogonality in a human embryonic kidney cell line (HEK293FT). Through transient transfection

<sup>1</sup>Department of Biomedical Engineering and Biological Design Center, Boston University, Boston, Massachusetts, USA. <sup>2</sup>Department of Biosystems Science and Engineering, ETH Zurich, Basel, Switzerland. <sup>3</sup>Department of Electrical and Computer Engineering, Boston University, Boston, Massachusetts, USA. Correspondence should be addressed to W.W.W. (wilwong@bu.edu).

Received 20 June 2016; accepted 27 January 2017; published online 27 March 2017; doi:10.1038/nbt.3805

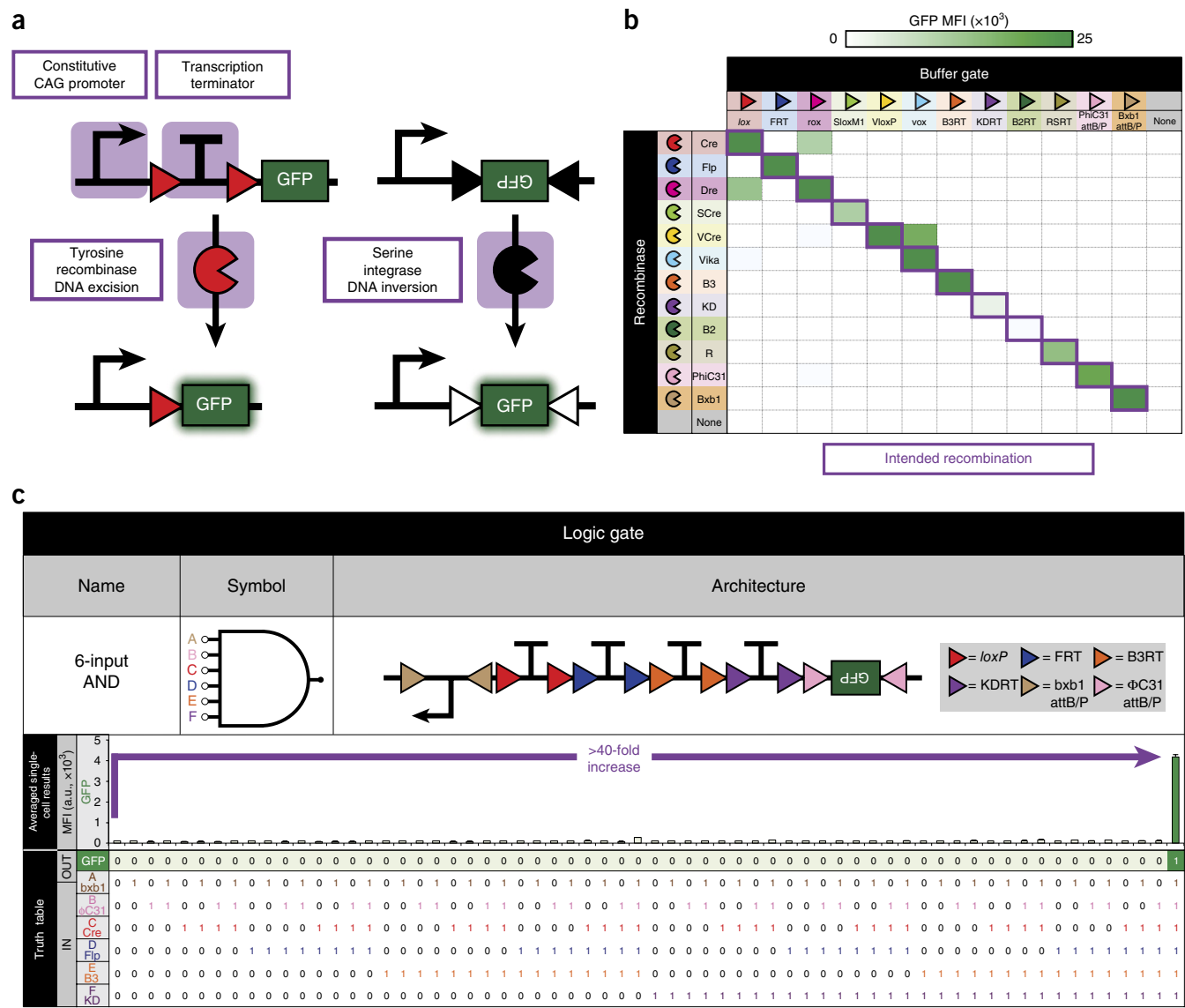


**Figure 1** Orthogonal site-specific tyrosine recombinases and serine integrases enable implementation of multi-input AND gates in mammalian cells. (a) Recombinases can perform simple BUF logic operations, either by tyrosine-recombinase-mediated excision (left) or serine-integrase-mediated inversion (right). (b) Recombinases are tested for their recombination efficiency and orthogonality on all BUF logic reporters. (c) A 6-input AND-gate that produces GFP when all inputs are present. MFI, mean fluorescence intensity from  $n = 3$  transfected cell cultures; a.u., arbitrary units. Error bars, s.e.m.

of cells with recombinases and their reporters (deletion-based BUF gates for tyrosine recombinases and inversion-based for serine integrases), ten of the enzymes were found to be highly active and sufficiently orthogonal to each other for our circuit design effort (Fig. 1b, Supplementary Fig. 1a, and Supplementary Table 1). It was found that recombinase expressional level could be tuned to minimize cross-talk between non-orthogonal recombinases (Supplementary Fig. 2). We focused our efforts on the use of Cre and Flp recombinases because of their prevalence in mammalian cell culture and animal experimentation.

Through an *ad hoc* design approach, we created all 16 possible 2-input Boolean logic gates by placing Cre and Flp recombination sites (*loxP* and FRT, respectively) around termination and coding sequences to yield the intended behaviors (Supplementary Fig. 3 and Supplementary Table 2). Due to the orthogonality of recombinases, it is possible to generate multi-input AND gates simply by placing

more termination sequences in tandem between a promoter and GFP. Indeed, we created a six-input AND gate that expresses GFP upon the excision of four termination sequences by tyrosine recombinases and the inversion of the EF1 $\alpha$  promoter and GFP by two serine integrases (Fig. 1c, Supplementary Fig. 1b, and Supplementary Table 3).

A key element that is required to implement more complex functions on a single transcriptional unit is the use of heterospecific recombination sites. Heterospecific sites, such as *loxP* and *lox2272*, differ from one another by only a few base pairs<sup>24</sup>, but they retain DNA excision capabilities in the presence of Cre, as long as two of the same sites are present, for example, *loxP* with *loxP*. We validated three sets of *lox* sites (*loxP*, *lox2272*, *loxN*), three sets of FRT (FRT, F3, F14), and Vlox (VloxP, Vlox2272), which demonstrated heterospecificity using Cre, Flp, and VCre enzymes, respectively (Supplementary Fig. 4 and Supplementary Table 4). This feature allows the excision of more than one non-connected region of DNA simultaneously,

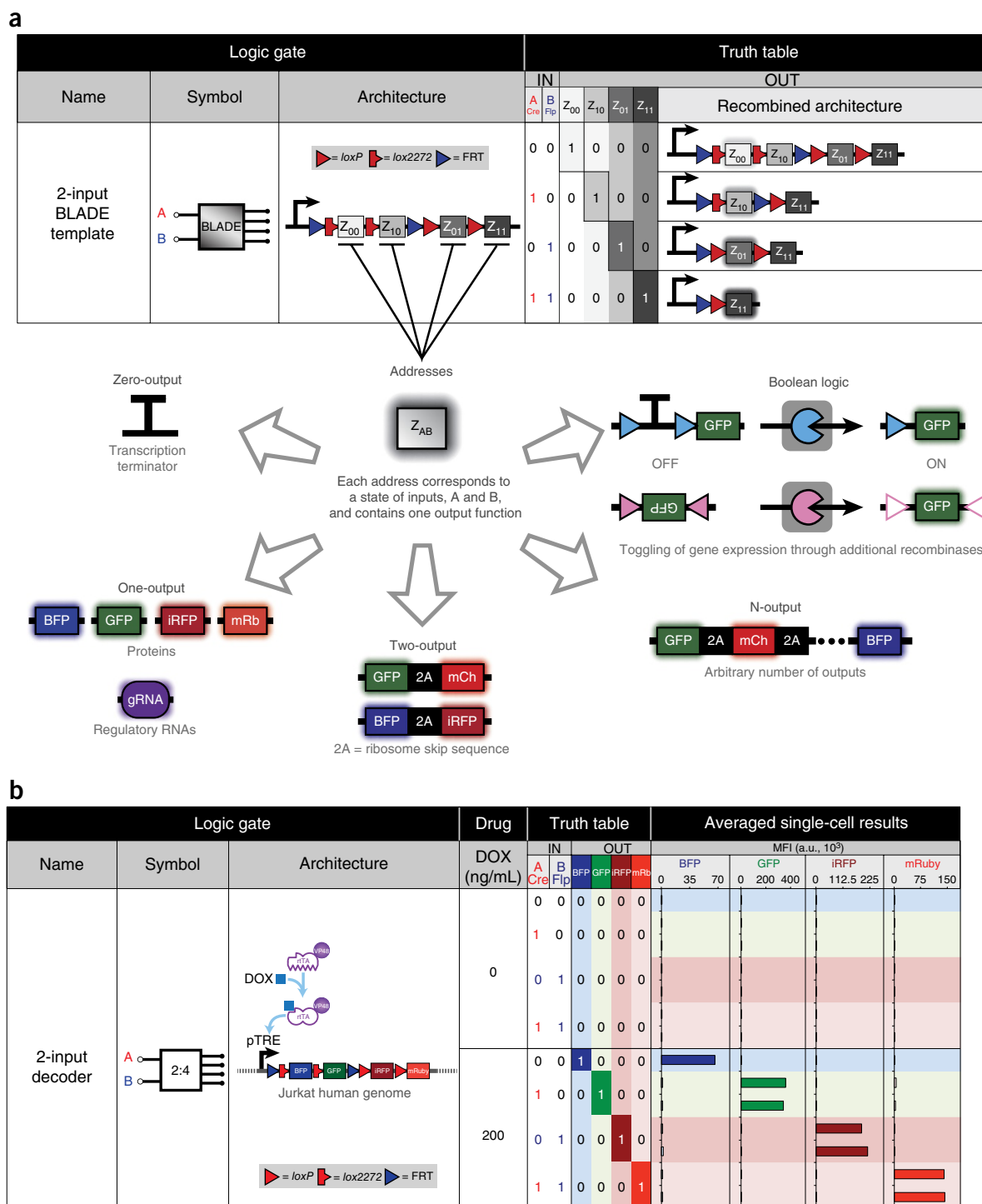


**Figure 2** 2-input BLADE platform can produce four distinct output functions based on two inputs. **(a)** 2-input BLADE template on one plasmid with a single transcriptional unit. This template contains four distinct regions of DNA (addresses) downstream of a promoter. Each address corresponds to an output function and is accessed or deleted via site-specific DNA recombination. Each address can be programmed from different configurations ranging from zero-inputs to Boolean functions. The first address ( $Z_{00}$ ), which is the closest to the promoter, corresponds to a state where no recombinase is expressed ( $A = 0, B = 0$ ). If the  $Z_{00}$  address contains a protein coding sequence, then that gene will be expressed. Gene expression from the other addresses downstream of  $Z_{00}$  will be blocked by the presence of the  $Z_{00}$  protein coding region. In the presence of recombinase A, which corresponds to state ( $A = 1, B = 0$ ), addresses  $Z_{00}$  and  $Z_{01}$  will be removed, thus moving address  $Z_{10}$  directly downstream of the promoter and allowing gene expression of address  $Z_{10}$  only to occur. Similarly, when only recombinase B is present ( $A = 0, B = 1$ ), addresses  $Z_{00}$  and  $Z_{10}$  are excised, allowing  $Z_{01}$  to be moved directly downstream of the promoter. Finally, when both recombinases are expressed ( $A = 1, B = 1$ ), addresses  $Z_{00}, Z_{01}, Z_{10}$  are all excised, thus placing  $Z_{11}$  downstream of the promoter unobstructed by the other addresses. **(b)** Integrated 2-input BLADE decoder with tagBFP, EGFP, iRFP720, and mRuby2 as addresses  $Z_{00}, Z_{10}, Z_{01}$ , and  $Z_{11}$  respectively. Plasmids constitutively expressing Cre and/or Flp are then stably integrated. Three days of doxycycline (DOX) treatment is used to permit the rtTA-VP48 protein to bind to the tetracycline response elements promoter (pTRE) to activate gene expression. Mean fluorescence intensity (MFI) is plotted of either  $n = 1$  or  $n = 2$  independent integrations. a.u., arbitrary units.

enabling encoding of logic on a single layer (recombinase inputs recombining with a single DNA strand reporter). This is juxtaposed to transcription-factor-based genetic logic, which necessitates cascading connections of multiple transcriptional responses; here, extensive fine-tuning is usually required to engineer functional circuits to balance input-output responses, which grows substantially as the number of inputs and outputs of the circuits increases.

### Single-layer multi-input recombinase-based design system

Although an *ad hoc* design approach can be successful in creating some recombinase-based circuits as others have demonstrated<sup>8,9,25–27</sup> and as we show here, a general strategy for producing any  $N$ -input- $M$ -output logic behavior has not, to our knowledge, been demonstrated before. BLADE exploits the features of site-specific recombinases to enable  $N$ -input- $M$ -output combinatorial computation in mammalian cells, where  $N$  and  $M$  can be any non-negative integer. Beyond the orthogonality of the recombinases and heterospecific sites, no further characterization of individual components is needed.

Each BLADE circuit is organized as a single transcriptional layer comprising a single promoter upstream of up to  $2^N$  regions of DNA sequences (or addresses,  $Z$ ), which are surrounded by recombination sites. Each BLADE circuit is designed such that when it is presented with recombinase inputs, addresses become transcriptionally active through excision of intervening regions between recombination sites downstream of the promoter. For example, a 2-input ( $N = 2$ ) BLADE circuit, which responds to inputs A and B, can accommodate up to  $2^2 = 4$  addresses with possible addresses being  $Z = Z_{AB} = Z_{00}, Z_{10}, Z_{01}$ , and  $Z_{11}$ , enumerating all combinatorial states of inputs A and B (Fig. 2a). The BLADE design is flexible with regards to the outputs that can be generated. Outputs can range from no transcriptional outputs (transcription terminator) at all, an arbitrary combination of outputs separated by ribosomal skip sequences (2A), Boolean functions like BUF that can toggle transcriptional responses ON or OFF through use of additional site-specific recombinases, or even other BLADE topologies. A BLADE design that utilizes  $2^N$  addresses permits creation of all possible  $N$ -input- $M$ -output combinatorial circuits and thus is necessary for implementing the most complex multi-input-multi-output truth tables<sup>28</sup>.

### A 2-input, 4-output circuit

For initial characterization of the 2-input BLADE system, single transcriptional output functions were tested. We constructed a 2-input, 4-output decoder circuit, which necessitates four addresses, each of which coincides with a distinct output: blue, green, infrared, and red fluorescent proteins (tagBFP, EGFP, iRFP720, and mRuby2, respectively) using a modular assembly strategy known as ‘unique nucleotide sequence-guided assembly’, based on Gibson isothermal assembly<sup>29,30</sup> (Fig. 2b and Supplementary Figs. 5–9). One advantage of the BLADE system is that expression of outputs is driven by a single promoter, thereby permitting additional control through the use of a drug-regulated promoter or encoding of further transcriptional logic. We demonstrated this principle by stable integration of a doxycycline-controlled decoder circuit into Jurkat T lymphocytes using *piggyBac*-mediated transposition. Jurkat T cells were chosen because they are an important suspension cell line for understanding T-cell signaling and easy to maintain during long-term passages. Constitutively expressed recombinases were then integrated into the genome. Following stable integration of the recombinases driven by constitutive promoters, doxycycline was used to regulate final output expression in a dose-dependent manner (Supplementary Fig. 10). This strategy provides a facile way of scaling the circuit response while maintaining the

logical functionality of the circuit. Furthermore, we showed that BLADE circuit functionality can be maintained for at least 2 weeks under varying doxycycline conditions (Supplementary Fig. 11). Moreover, the decoder circuit performed as predicted through transient transfection of HEK293FT cells with strong fluorescent protein expression for each state of inputs (Supplementary Fig. 12 and Supplementary Table 5). HEK293FT was chosen here (and for subsequent experiments) because they enable high-throughput experimentation owing to the inexpensive and highly efficient polyethylenimine transfection reagent.

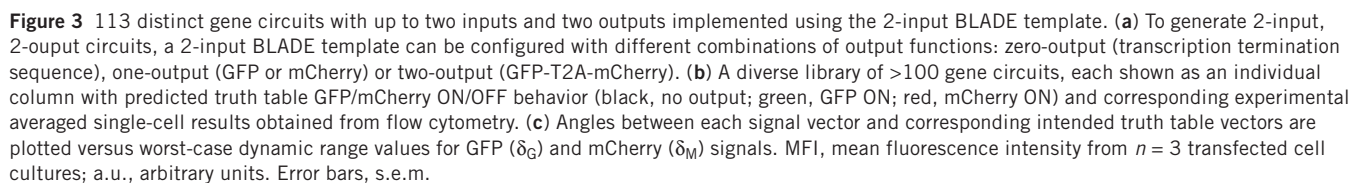
### Scaling-up and quantitation of circuit design

To test the robustness of the BLADE system on a large scale, we produced the largest, to the best of our knowledge, collection of functionally unique logic circuits in mammalian cells (a library of 113 circuits with up to two inputs and outputs (Fig. 3, Supplementary Fig. 13, and Supplementary Data 1)). This set contains two 2-input circuits: the half adder (gate 104) and half subtractor (gate 99), which perform 2-input arithmetic and are widely used and studied in electronics. Whereas all 113 circuits were qualitatively observed to implement the correct computation, we quantified their functional correctness using a novel vector proximity (VP) metric measuring the misalignment between a circuit’s biological implementation and its ideal implementation from its intended truth table (Supplementary Code). Truth tables and obtained experimental results were represented as vectors, ‘truth table’ and ‘signal vectors’, respectively, in an eight-dimensional vector space. The angular error between these two vectors (VP angle metric) was calculated with  $0^\circ$ , meaning the data represent the intended truth table perfectly, and  $90^\circ$ , meaning the data demonstrate completely incorrect output (inverted response to the intended truth table). The VP angle metric shows that 93.8% (106/113) of the circuits had an angle no more than  $15^\circ$ , and none had an angle of more than  $25^\circ$  from their ideal implementation.

We extended the VP measure of correctness to obtain a quantitative and discrete test of whether an implemented circuit is correct or incorrect. For any implemented circuit we measured its VP angle from all possible truth tables, and sorted the results in ascending order. We defined the rank of the intended truth table in this sorted list as the circuit’s VP global rank. We call a circuit functionally valid under this measure if it has the best (that is, smallest) VP global rank. For our library of 113 circuits, we calculated the VP angle between each signal vector and all 255 (up to 2-input, up to 2-output, excluding the 0-input, 0-output FALSE) truth table vectors. Global rank values were determined according to how many truth table vectors had lower VP angles than the intended truth table vector. We found that 96.5% (109/113) of the tested circuits gave the lowest angle between their signal vector (global rank = 0/255) and their intended truth table vectors (Supplementary Figs. 14 and Supplementary Table 6). This success rate of 96.5% is the highest reported, to our knowledge, for large-scale circuit construction in mammalian cells. Only four circuits had a global rank of 1, meaning there was only one other truth table that yielded a lower VP angle; no circuits had a rank more than 1. To facilitate data sharing and further analysis by other researchers, we have developed an interactive website (<http://datasheets.synbiotools.org>) that contains the data of all of our 113 circuits summarized in a datasheet format<sup>31</sup>.

### Reprogrammable combinatorial logic

One important class of circuits found in electronics is field-programmable, read-only memory (FPRM). The input-output behavior of these circuits can be configured in the field after





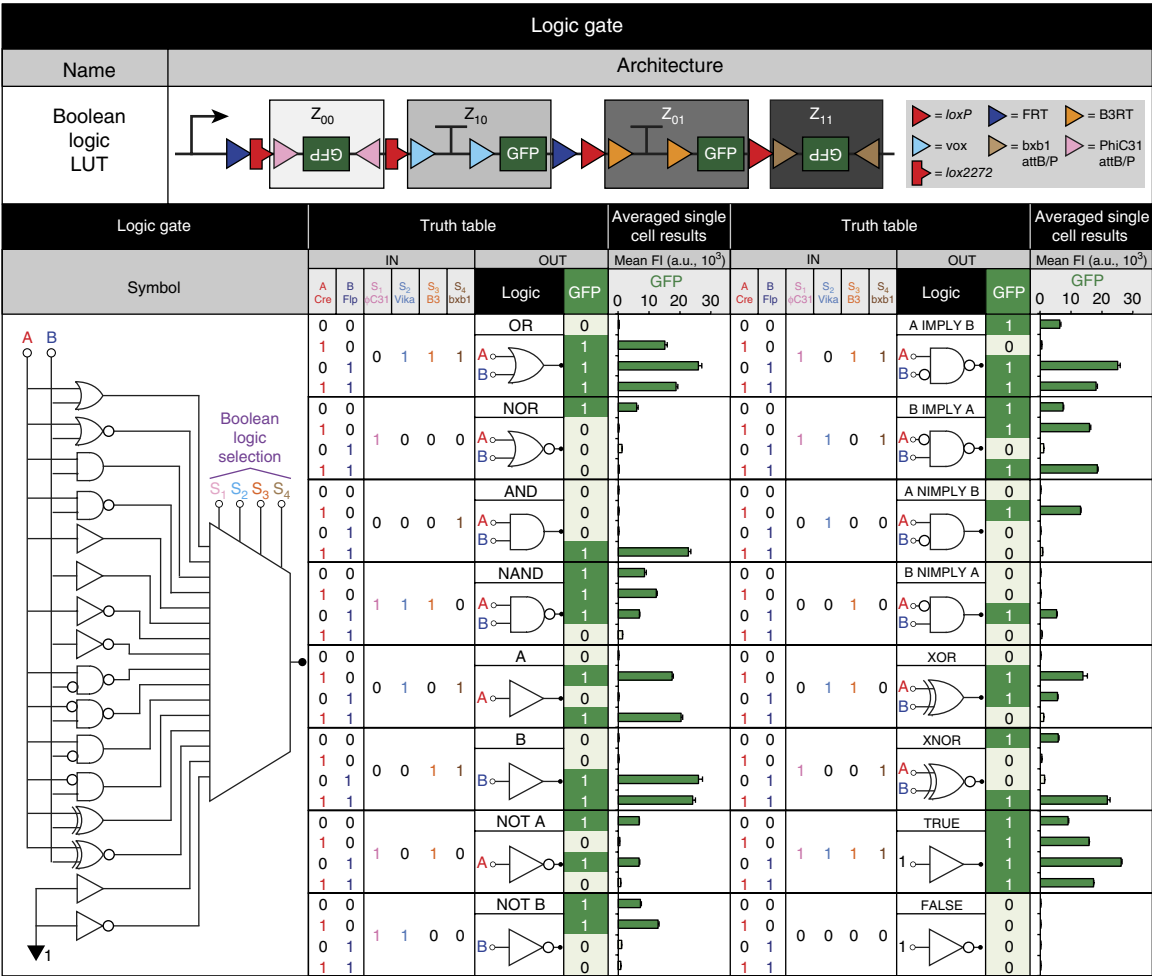


**Figure 4** Field-programmable storage and retrieval of logic and memory using a Boolean logic look-up table (LUT). The Boolean logic LUT is a 6-input-one-output genetic circuit that receives two data inputs, A and B, and is controlled by four select inputs, S<sub>1</sub>, S<sub>2</sub>, S<sub>3</sub>, and S<sub>4</sub>, producing an output of GFP. The select inputs are used to change data input-output behavior; each combination configures the circuit to any of the 16 Boolean logic gates. FI, fluorescence intensity from  $n = 3$  independent transfections. Error bars, s.e.m.

manufacturing, allowing users to program the function computed by the circuit at a later time. We built a genetic FPRM circuit for living cells termed a Boolean logic look-up table that is based on placing BUF gates into the four addresses of the 2-input BLADE template (Fig. 4, Supplementary Fig. 15, and Supplementary Table 7). This circuit has two data inputs, A and B, and four select inputs, S<sub>1</sub>, S<sub>2</sub>, S<sub>3</sub>, and S<sub>4</sub>. Each select input can control which buffer gates are transcriptionally active or not (GFP ON or OFF). Thus, each combination of select inputs configures the circuit to 1 of 16 possible Boolean logic gates with up to two inputs and one output. For instance, an OR function can be achieved using select inputs S<sub>2</sub>, S<sub>3</sub>, and S<sub>4</sub>, keeping address Z<sub>00</sub> GFP OFF and setting addresses Z<sub>10</sub>, Z<sub>01</sub>, and Z<sub>11</sub> GFP ON. Thus, this circuit allows one to reconfigure the computation within living cells without requiring additional DNA assembly. This circuit behaves as expected in HEK293FT cells. To illustrate the flexibility of our system in terms of recombinase choices, we created an alternative Boolean logic look-up table (Supplementary Fig. 16).

### Arithmetic operations using BLADE

Extending the BLADE framework further, we developed a 3-input BLADE template for constructing sophisticated arithmetic functions

in human cells (Fig. 5a, Supplementary Figs. 17, and 18). This template responds to three inputs (Cre, Flp, and VCre) and contains eight addresses for expression of up to eight distinct transcriptional outputs. This design utilizes three different heterospecific sites for Cre and Flp, but just one site for VCre. Three 3-input-2-output arithmetic computational circuits were made and tested in HEK293FT cells from the 3-input BLADE template (Fig. 5b, Supplementary Fig. 19, and Supplementary Table 8). The full adder and full subtractor can perform either binary addition or subtraction of three 1-bit inputs, respectively. Furthermore, the half adder–subtractor is an arithmetic FPRM circuit that can compute addition or subtraction on two data inputs, A and B, depending on the presence of one select input C. BLADE templates with more than three inputs can be generated by using additional recombinases and heterospecific recombination sites that follow a simple recursive design algorithm where recombinase switches are nested within each other, yielding designs for implementing any  $N$ -input combinatorial logic function (Supplementary Fig. 20). This non-intensive computational approach produces designs with the total number of recombination site pairs for  $N$ -inputs being  $2^N - 1$ , for  $N \geq 0$ ; this is consistent with the  $2^N$  rows needed to specify the truth table of an  $N$ -input function.

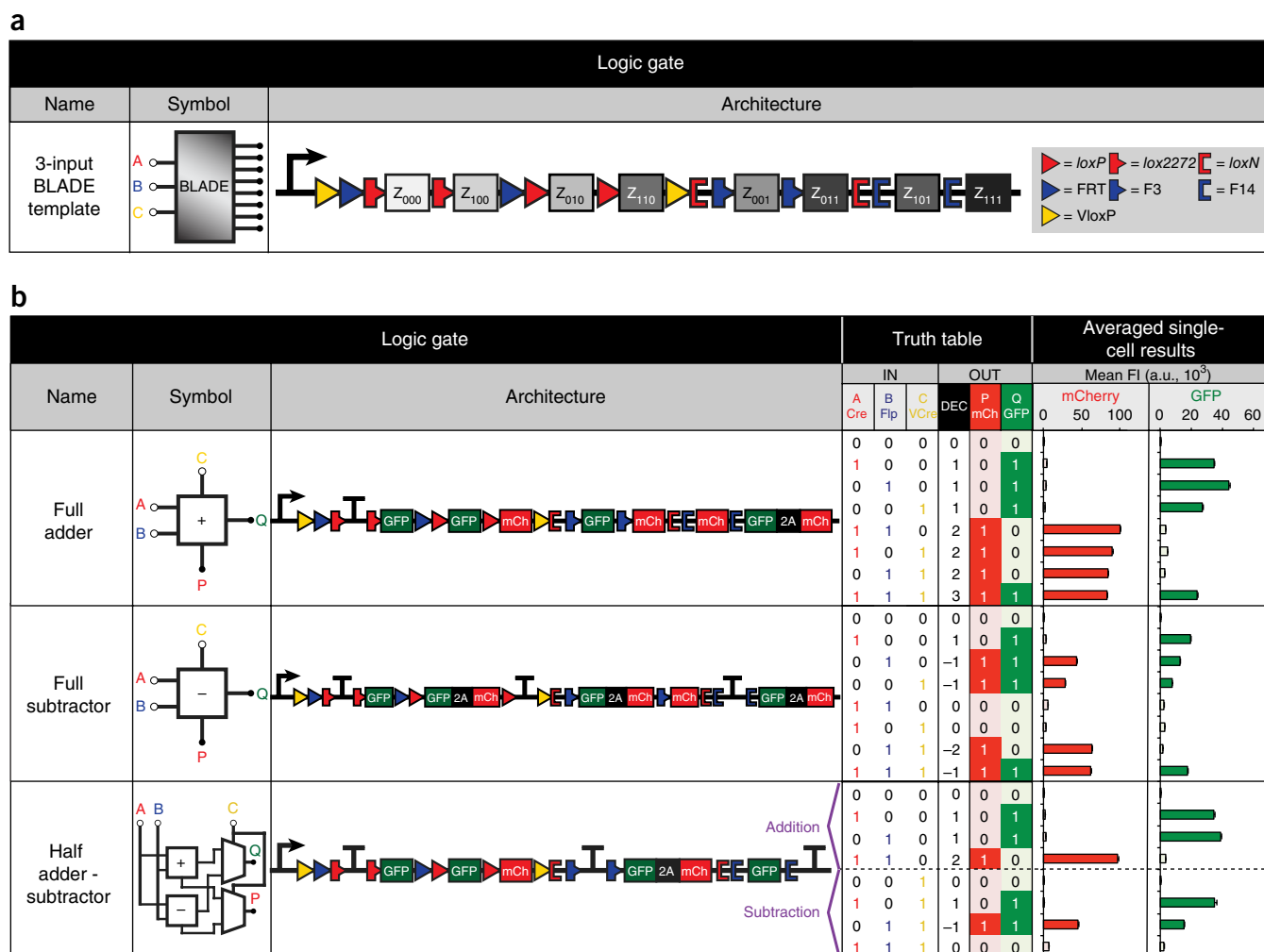


**Figure 5** A 3-input BLADE template can be applied to create 3-input arithmetic computational circuits. **(a)** The 3-input BLADE template can receive up to three inputs and produce eight distinct output functions. **(b)** Three 3-input-2-output binary arithmetic computational circuits made using the 3-input BLADE template. The full adder can add  $A + B + C$  while the full subtractor calculates  $A - B - C$ . For addition, input C, output P, and output Q represent Carry In, Carry Out, and Sum, respectively. For subtraction, input C, output P, and output Q signify Borrow In, Borrow Out, and Difference, respectively. The half adder-subtractor performs either binary addition of  $A + B$  or binary subtraction of  $A - B$ , depending on the presence of select input C. FI, fluorescence intensity from  $n = 3$  transfected cell cultures; a.u. = arbitrary units. Error bars, s.e.m.

### Small-molecule inputs for BLADE

Next, we interfaced the BLADE system with biochemically relevant inputs. To induce Cre recombination, an  $ERT^2$ -Cre- $ERT^2$  construct was used whereby a mutated estrogen receptor ( $ERT^2$ ) secludes Cre recombinase activity from the nucleus unless a small-molecule 4-hydroxytamoxifen (4OHT) is added, which permits translocation of the fusion protein to the nucleus. For Flp induction, a split Flp system was developed that induces Flp recombinase activity upon phytohormone abscisic acid (ABA)-induced heterodimerization (Fig. 6a, Supplementary Fig. 21, and Supplementary Table 9). Logical detection of these two small-molecule inputs was successful using the 2-input BLADE decoder with minimal leaky recombinase behavior in HEK293FT cells. Logic induction dynamics were characterized over the course of 48 h, which revealed early encoding of logic and introduction of leaky recombinase behavior toward the end of the time course (Supplementary Figs. 22, 23, and 24). A BLADE decoder affords the ability to combinatorially select an exponential number of DNA regions (e.g., eight regions via three inputs), which is advantageous for the limited set of eukaryotic inducible systems.

### CRISPR-Cas9 combined with BLADE

To test whether the BLADE system can be used to regulate endogenous mammalian gene expression, we interfaced it with the CRISPR-Cas9 system using recombinase-based excision of guide RNA (gRNA) sequences. We first tested whether recombination sites or cloning scar DNA sequences would affect the activity of a Cas9 transcription activator (dCas9-VPR), as these sequences would be directly coded into RNA fused to the gRNA. We found that these sequences (up to 136 bases) added to the 5' end of the gRNA had no detrimental effect on transcription activation of a mCherry reporter plasmid (Supplementary Fig. 25). Next, the 2-input decoder was rebuilt to use an RNA polymerase III human U6 promoter and guide RNAs (gRNAs) as addresses that target promoters of four human endogenous genes (*NGN2* (also known as *NEUROG2*), *MIAT*, *ACTC1*, and *TTN*). These targets were chosen because of their documented efficient gRNA activity<sup>32</sup>. This CRISPR-based 2-input decoder system was used for the transfection along with a Cas9 transcription activator (dCas9-VPR)<sup>32</sup>, and recombinase activities were induced with 4OHT and ABA (Fig. 6b and Supplementary Tables 10 and 11). At the completion of the transient transfection of

HEK293FT cells, mRNA fold-changes of the target endogenous genes were determined using quantitative real-time PCR and corresponded to the 2-input decoder truth table logic. Owing to the easy programmability

of the CRISPR–Cas9 system, this system will be very useful for genome-wide transcriptional reprogramming studies, entailing unprecedented control of endogenous human genes and cell states.

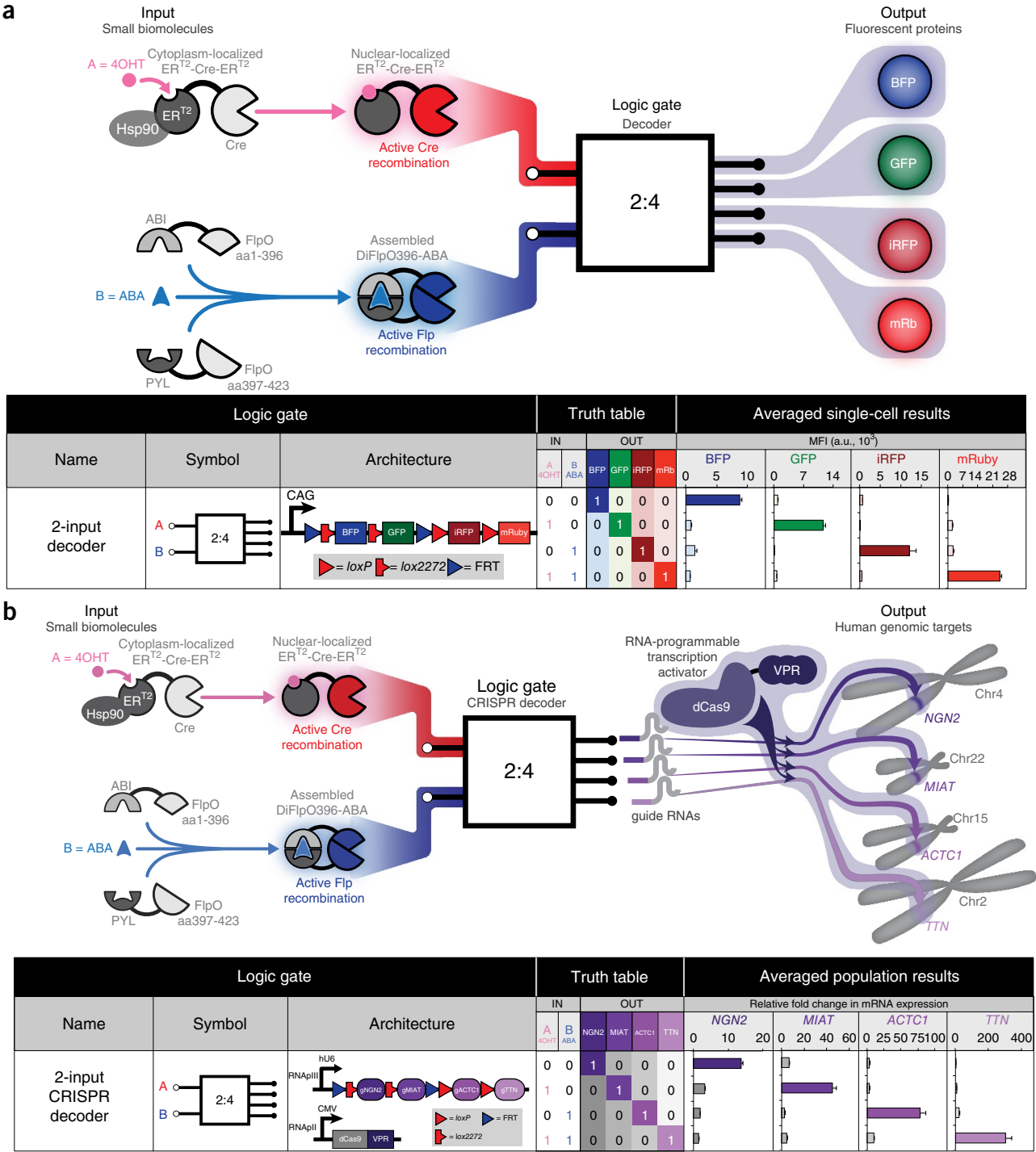


**Figure 6** Interfacing BLADE with biologically relevant inputs and outputs. (a) Small molecules, 4-hydroxytamoxifen (4OHT), and abscisic acid (ABA) are used to induce Cre and Flp recombination activities, respectively, on a decoder circuit containing four fluorescent protein outputs. Chemical induction of Cre recombination is achieved through 4OHT-mediated translocation of a Cre protein fused to mutated estrogen nuclear receptors (ER<sup>T2</sup>) from the cytoplasm to the nucleus. Chemical induction of Flp recombination is achieved through a split Flp recombinase construct fused to ABA-binding domains ABI and PYL. Mean fluorescence intensity (MFI) is plotted from  $n = 3$  transfected cell cultures; error bars indicate the s.e.m. (b) Small molecules, 4OHT and ABA, are used to induce Cre and Flp recombination activities on a decoder circuit interfaced with a dCas9-VPR (VP64, p65, Rta) transcription activator. Four human genomic promoters are targets for activation via association of corresponding guide RNAs (gRNA) with dCas9-VPR. Total RNA was collected, and averaged relative fold-changes in target mRNA expression were obtained through quantitative real-time PCR of  $n = 3$  transfected cell cultures. Error bars, s.e.m.



## DISCUSSION

The BLADE system can generate multiple, complex genetic circuits. We used BLADE to build >100 functionally distinct circuits, most of which have never, to our knowledge, been documented before in any living organism.

Most of our circuits had the intended logic, as quantified by the VP metrics that we devised to quantitate their performance. BLADE can be used to regulate mRNA and gRNA expression, too. When combined with drug-inducible control of recombinase activity, we were able to conditionally regulate gene expression and cell states. We created a split FLP protein whose activity can be reconstituted with chemically inducible dimerization systems. This split FLP configuration could be valuable to animal geneticists to complement existing Cre systems. Furthermore, we showed that BLADE works in different cell types including embryonic kidney and Jurkat T cells. Key attributes of the BLADE system are summarized in **Supplementary Table 12**.

Composition of simple gates into large hierarchies of modules has been successful in electronic circuit design because components are physically separated from each other, allowing reuse of well-characterized and high-performing parts. This has enabled computing circuits with extremely predictable behaviors to be built. However, applying an electrical engineering strategy to synthetic biology has proven difficult owing to an incomplete understanding of how different components behave when connected together in a single cell<sup>17,33</sup>, even when the components are designed to be ‘plug and play’. As a result, aside from selected examples<sup>14,34</sup>, only a handful of synthetic multi-input-multi-output circuits have been reported.

Furthermore, a multi-layer circuit design requires orthogonal biological ‘wires’ to link each layer, and these wires have unpredictable properties. In order to solve this problem, much effort has been devoted to parts development<sup>35,36</sup> at the expense of circuit design. Detailed characterization of components, together with standards and design automation programs may improve predictability of the interoperability of different parts<sup>18,31</sup>.

The BLADE system is enabled by the unique chemistry of recombinases (DNA rearrangement). The same recombinase can activate and inhibit gene expression simultaneously in the same transcription unit with equal efficiency, a feature that is very difficult to accomplish with transcription factors. This feature allowed us to design the BLADE system in a single layer (single transcription unit) to implement any combinatorial Boolean logic, provided that a sufficient number of recombinases and heterospecific sites are available.

We define the number of layers in a computing circuit as the maximum number of states along the shortest path in any computation. By ‘single-layer’, we connote the following property unique to BLADE designs. Unlike other circuit architectures, there is no need for a ‘molecular wire’ to communicate the results of a sub-computation in one part of the circuit to any other part of the circuit: the inputs themselves communicate information throughout a computation. Our single-layer BLADE system requires only a few proteins to carry out a large set of complex logical operations in mammalian cells. Single-layer circuits do not need the output signal levels of one gate to be tuned, or matched, to the input signal levels of another. One trade-off of a single-layer design is that the performance of a circuit cannot be predicted based on the property of its components.

Some circuits did not pass our stringent VP global rank metric evaluation; however, all circuits yielded results that had close alignment with their intended truth table. A potential source of underperformance could arise from interference of recombinase site sequences on ribosome activities (e.g., hair-pinning hampering translation initiation or cryptic translation initiation sequences). The RNA Pol

III/CRISPR-based BLADE system could be an attractive circuit design to explore since gRNA or other regulatory RNA outputs are not subjected to translation-based failure modes.

Transcription-factor-based genetic circuits have been widely adopted in synthetic circuit designs<sup>18,37–39</sup> because natural genetic circuits, which often serve as the inspiration for synthetic circuit designs, are mainly implemented using transcription factors. Only a few microbial pathways use recombinases (e.g., fim invertase in *Escherichia coli*)<sup>40,41</sup>. Unlike transcription-factor-based circuits, recombinase-based circuits are single-use systems, which cannot monitor dynamic input signals. However, recombinases are particularly useful for engineering logic behaviors. Furthermore, upon integration into a genome, recombinase-based systems can provide stable memory and have been used in numerous experiments, such as in tissue-specific gene expression experiments in which memory of tissue- or condition-specific inputs that result in sustained gene expression (or knockout) is desirable. In addition, serine integrases have been used to develop temporal logic state machines in bacteria in which the circuits sense and ‘remember’ the order in which signal inputs occur<sup>42,43</sup>. It is conceivable that those designs could be refactored to function in mammalian cells. It is also possible to modify the BLADE system to carry out temporal logic computations, thus enabling the use of the more widely adopted tyrosine recombinases in a single-layer circuit topology. The prevalence of recombinases in different systems and organisms shows that single-use systems are often sufficient for biomedical or biotechnological applications<sup>23,44</sup>.

Genome mining has been performed to uncover and test a large set of serine integrases<sup>45</sup>, and many putative recombinases remain to be characterized from structural identification in genome sequence databases. Furthermore, efforts have been made to design and implement recombinases that can be made to recombine different DNA sequences through fusion of recombinase catalytic domains to programmable DNA-binding proteins, such as zinc finger, transcription activator-like effector (TALE), and Cas9 sequences<sup>46–48</sup>; generation of chimeric recombinases<sup>49</sup>; or alteration of specificity through molecular evolution experiments<sup>50</sup>. Therefore, we envision that an unlimited set of recombinase parts are likely available for incorporation with BLADE to create biocomputation circuits with unprecedented sophistication.

## METHODS

Methods, including statements of data availability and any associated accession codes and references, are available in the [online version of the paper](#).

*Note: Any Supplementary Information and Source Data files are available in the online version of the paper.*

## ACKNOWLEDGMENTS

B.H.W. acknowledges funding from the NSF Graduate Research Fellowship Program (DGE-1247312) and an NIH/NIGMS fellowship (T32-GM008764). S.B. was supported in part by the National Science Foundation Expeditions in Computing Award No. 1522074, which is part of the “Living Computing Project” (<https://www.programmingbiology.org/>). W.W.W. acknowledges funding from the NIH Director’s New Innovator Award (1DP2CA186574), NSF Expedition in Computing (1522074), NSF CAREER (162457), NSF BBSRC (1614642), and Boston University College of Engineering Dean’s Catalyst Award. We thank C. Bashor, D. Chakravarti, N. Patel, and S. Slomovic for suggestions on the manuscript; A. Belkina and T. Haddock for flow cytometry assistance; J. Torella for help with UNS-guided assembly; and M. Park and J. Eyckmans for RT-qPCR assistance. A. Nagy for the kind gift of the Dre construct.

## AUTHOR CONTRIBUTIONS

B.H.W. made molecular and cellular reagents, performed experiments, analyzed data and generated all figures. S.B. conceived the vector proximity analyses for

circuit performance and developed the datasheets attribution and website. B.H.W. and S.B. developed and performed the vector proximity analyses. L.D.C., N.T.H.P., T.L., and A.E. made molecular and cellular reagents and performed preliminary experiments. B.H.W. and W.W.W. conceived the project. B.H.W., S.B., and W.W.W. wrote the paper. All authors commented on and approved the paper.

#### COMPETING FINANCIAL INTERESTS

The authors declare competing financial interests: details are available in the [online version of the paper](#).

Reprints and permissions information is available online at <http://www.nature.com/reprints/index.html>.

Publisher's note: Springer Nature remains neutral with regard to jurisdictional claims in published maps and institutional affiliations.

- Khalil, A.S. & Collins, J.J. Synthetic biology: applications come of age. *Nat. Rev. Genet.* **11**, 367–379 (2010).
- Wei, P. *et al.* Bacterial virulence proteins as tools to rewire kinase pathways in yeast and immune cells. *Nature* **488**, 384–388 (2012).
- Roybal, K.T. *et al.* Precision tumor recognition by T cells with combinatorial antigen-sensing circuits. *Cell* **164**, 770–779 (2016).
- Chakravarti, D. & Wong, W.W. Synthetic biology in cell-based cancer immunotherapy. *Trends Biotechnol.* **33**, 449–461 (2015).
- Xie, M. *et al.*  $\beta$ -cell-mimetic designer cells provide closed-loop glycemic control. *Science* **354**, 1296–1301 (2016).
- Slomovic, S. & Collins, J.J. DNA sense-and-respond protein modules for mammalian cells. *Nat. Methods* **12**, 1085–1090 (2015).
- Courbet, A., Endy, D., Renard, E., Molina, F. & Bonnet, J. Detection of pathological biomarkers in human clinical samples via amplifying genetic switches and logic gates. *Sci. Transl. Med.* **7**, 289ra83 (2015).
- Fenno, L.E. *et al.* Targeting cells with single vectors using multiple-feature Boolean logic. *Nat. Methods* **11**, 763–772 (2014).
- Madisen, L. *et al.* Transgenic mice for intersectional targeting of neural sensors and effectors with high specificity and performance. *Neuron* **85**, 942–958 (2015).
- Ro, D.K. *et al.* Production of the antimalarial drug precursor artemisinic acid in engineered yeast. *Nature* **440**, 940–943 (2006).
- Bogorad, I.W., Lin, T.S. & Liao, J.C. Synthetic non-oxidative glycolysis enables complete carbon conservation. *Nature* **502**, 693–697 (2013).
- Gaber, R. *et al.* Designable DNA-binding domains enable construction of logic circuits in mammalian cells. *Nat. Chem. Biol.* **10**, 203–208 (2014).
- Xie, Z., Wroblewska, L., Prochazka, L., Weiss, R. & Benenson, Y. Multi-input RNAi-based logic circuit for identification of specific cancer cells. *Science* **333**, 1307–1311 (2011).
- Guinn, M. & Bleris, L. Biological 2-input decoder circuit in human cells. *ACS Synth. Biol.* **3**, 627–633 (2014).
- Weber, W. *et al.* A synthetic time-delay circuit in mammalian cells and mice. *Proc. Natl. Acad. Sci. USA* **104**, 2643–2648 (2007).
- Regot, S. *et al.* Distributed biological computation with multicellular engineered networks. *Nature* **469**, 207–211 (2011).
- Brophy, J.A. & Voigt, C.A. Principles of genetic circuit design. *Nat. Methods* **11**, 508–520 (2014).
- Nielsen, A.A. *et al.* Genetic circuit design automation. *Science* **352**, aac7341 (2016).
- Appleton, E., Tao, J., Haddock, T. & Densmore, D. Interactive assembly algorithms for molecular cloning. *Nat. Methods* **11**, 657–662 (2014).
- Rodrigo, G. & Jaramillo, A. AutoBioCAD: full biodesign automation of genetic circuits. *ACS Synth. Biol.* **2**, 230–236 (2013).
- Huynh, L., Kececioglu, J., Köppe, M. & Tagkopoulos, I. Automatic design of synthetic gene circuits through mixed integer non-linear programming. *PLoS One* **7**, e35529 (2012).
- Stanton, B.C. *et al.* Genomic mining of prokaryotic repressors for orthogonal logic gates. *Nat. Chem. Biol.* **10**, 99–105 (2014).
- Nagy, A. Cre recombinase: the universal reagent for genome tailoring. *Genesis* **26**, 99–109 (2000).
- Lee, G. & Saito, I. Role of nucleotide sequences of loxP spacer region in Cre-mediated recombination. *Gene* **216**, 55–65 (1998).
- Siuti, P., Yazbek, J. & Lu, T.K. Synthetic circuits integrating logic and memory in living cells. *Nat. Biotechnol.* **31**, 448–452 (2013).
- Bonnet, J., Yin, P., Ortiz, M.E., Subsoontorn, P. & Endy, D. Amplifying genetic logic gates. *Science* **340**, 599–603 (2013).
- Schönhuber, N. *et al.* A next-generation dual-recombinase system for time- and host-specific targeting of pancreatic cancer. *Nat. Med.* **20**, 1340–1347 (2014).
- Shannon, C.E. The synthesis of two-terminal switching circuits. *Bell Syst. Tech. J.* **28**, 59–98 (1949).
- Torella, J.P. *et al.* Rapid construction of insulated genetic circuits via synthetic sequence-guided isothermal assembly. *Nucleic Acids Res.* **42**, 681–689 (2014).
- Torella, J.P. *et al.* Unique nucleotide sequence-guided assembly of repetitive DNA parts for synthetic biology applications. *Nat. Protoc.* **9**, 2075–2089 (2014).
- Canton, B., Labno, A. & Endy, D. Refinement and standardization of synthetic biological parts and devices. *Nat. Biotechnol.* **26**, 787–793 (2008).
- Chavez, A. *et al.* Highly efficient Cas9-mediated transcriptional programming. *Nat. Methods* **12**, 326–328 (2015).
- Jayanthi, S., Nilgiriwala, K.S. & Del Vecchio, D. Retroactivity controls the temporal dynamics of gene transcription. *ACS Synth. Biol.* **2**, 431–441 (2013).
- Ausländer, S., Ausländer, D., Müller, M., Wieland, M. & Fussenegger, M. Programmable single-cell mammalian biocomputers. *Nature* **487**, 123–127 (2012).
- Khalil, A.S. *et al.* A synthetic biology framework for programming eukaryotic transcription functions. *Cell* **150**, 647–658 (2012).
- Green, A.A., Silver, P.A., Collins, J.J. & Yin, P. Toehold switches: de-novo-designed regulators of gene expression. *Cell* **159**, 925–939 (2014).
- Gardner, T.S., Cantor, C.R. & Collins, J.J. Construction of a genetic toggle switch in *Escherichia coli*. *Nature* **403**, 339–342 (2000).
- Stricker, J. *et al.* A fast, robust and tunable synthetic gene oscillator. *Nature* **456**, 516–519 (2008).
- Elowitz, M.B. & Leibler, S. A synthetic oscillatory network of transcriptional regulators. *Nature* **403**, 335–338 (2000).
- Johnson, R.C. in *Mobile DNA II* (eds. Craig, N., Craigie, R., Gellert, M. & Lambowitz, A.) 230–271 (American Society of Microbiology, 2002).
- Blomfield, I.C. The regulation of pap and type 1 fimbriation in *Escherichia coli*. *Adv. Microb. Physiol.* **45**, 1–49 (2001).
- Roquet, N., Soleimany, A.P., Ferris, A.C., Aaronson, S. & Lu, T.K. Synthetic recombinase-based state machines in living cells. *Science* **353**, aad8559 (2016).
- Hsiao, V., Hori, Y., Rothmund, P.W. & Murray, R.M. A population-based temporal logic gate for timing and recording chemical events. *Mol. Syst. Biol.* **12**, 869 (2016).
- Branda, C.S. & Dymecki, S.M. Talking about a revolution: The impact of site-specific recombinases on genetic analyses in mice. *Dev. Cell* **6**, 7–28 (2004).
- Yang, L. *et al.* Permanent genetic memory with >1-byte capacity. *Nat. Methods* **11**, 1261–1266 (2014).
- Mercer, A.C., Gaj, T., Fuller, R.P. & Barbas, C.F. III. Chimeric TALE recombinases with programmable DNA sequence specificity. *Nucleic Acids Res.* **40**, 11163–11172 (2012).
- Sirk, S.J., Gaj, T., Jonsson, A., Mercer, A.C. & Barbas, C.F. III. Expanding the zinc-finger recombinase repertoire: directed evolution and mutational analysis of serine recombinase specificity determinants. *Nucleic Acids Res.* **42**, 4755–4766 (2014).
- Chaikind, B., Bessen, J.L., Thompson, D.B., Hu, J.H. & Liu, D.R. A programmable Cas9-serine recombinase fusion protein that operates on DNA sequences in mammalian cells. *Nucleic Acids Res.* **44**, 9758–9770 (2016).
- Shaikh, A.C. & Sadowski, P.D. Chimeras of the Flp and Cre recombinases: tests of the mode of cleavage by Flp and Cre. *J. Mol. Biol.* **302**, 27–48 (2000).
- Karpinski, J. *et al.* Directed evolution of a recombinase that excises the provirus of most HIV-1 primary isolates with high specificity. *Nat. Biotechnol.* **34**, 401–409 (2016).

## ONLINE METHODS

**DNA assembly.** All constructs were transformed and maintained in Top10 *Escherichia coli* competent cells (Life Technologies) at 37 °C or 30 °C before miniprep (Epoch Life Sciences) or midiprep (Macherey Nagel). All plasmids were created using standard molecular biology practices of ligation, digestion and transformation, in addition to Gibson isothermal assembly and Unique Nucleotide Sequence (UNS) Guided assembly (a modular extension of Gibson assembly), where DNA fragments that are to be connected to each other are flanked by short homology sequences and are then fused together by a one-pot isothermal digestion, polymerization, and ligation reaction. This latter strategy permits a modular, easy, efficient, and fast framework for construction of DNA. In UNS-guided assembly, the homology sequences have been standardized (e.g., U1, U2, U3...UX) and have been computationally optimized for proper assembly (reduction of hairpins, sequence homology, and GC tracts) and ease of use (no start codons or useful restriction sites). Genetic cassettes that are to be connected are cloned into part vectors, which contain the UNSes that surround the insert. Part vectors are then sequenced-verified using Sanger sequencing (Quintara Biosciences). Restriction digests and gel purifications are then performed to isolate the cassettes flanked with the UNSes. Finally, these products are joined to a linearized destination vector via Gibson isothermal assembly. For the 113 circuits displayed in **Figure 3**, analytical PCRs were performed to verify inserts were assembled correctly through amplifications across the UNS sequences. Construction details are elaborated in **Supplementary Figs. 5, 7 and 18**.

**Maintenance and transient DNA transfection of HEK293FT cells.** DNA was transfected into the human embryonic kidney cell line (HEK293FT) using a polyethylenimine (PEI) protocol. Cells were plated onto 48- (250 µL) or 96-well (100 µL) plates the day before transfection (200,000 cells/mL), such that the cells were 50–70% confluent the day of transfection. Cells were kept in a humidified incubator at 37 °C and 5% CO<sub>2</sub> and maintained in DMEM medium (Corning) with 10% heat-inactivated fetal bovine serum (Life Technologies), 50 UI/mL penicillin, 50 µg/mL streptomycin (Corning), 2 mM glutamine (Corning) and 1 mM sodium pyruvate (Lonza). PEI stocks were made from linear polyethylenimine (Polysciences 23966-2) and were dissolved at a concentration of 0.323 g/L in deionized water with the assistance of concentrated hydrochloric acid and sodium hydroxide and then sterilized through filtration (0.22 µm). PEI stocks were stored at –80 °C until use and warmed to room temperature before usage. For 48-well plate transfections, DNA (1,000 ng, 50 ng/µL) was dissolved and brought up to a volume of 50 µL using 0.15 M sodium chloride (NaCl, Fisher Scientific). DNA-NaCl solutions were then mixed with 50 µL of a PEI-NaCl mixture (8 µL PEI: 42 µL NaCl). These solutions were then incubated at room temperature for 10 min, and 25 µL was carefully dropped into individual wells of HEK293FT cells (250 ng DNA/well). Similarly, for 96-well-plate transfections, DNA (500 ng, 50 ng/µL) was dissolved and brought up to a volume of 25 µL using 0.15 M sodium chloride (NaCl). DNA-NaCl solutions were then mixed with 25 µL of a PEI-NaCl (4 µL PEI: 21 µL NaCl) mixture. These solutions were then incubated at room temperature for 10 min, and 10 µL was carefully dropped into individual wells of HEK293FT cells (100 ng DNA/well). Electronic space-adjustable multichannel pipettors (Integra Biosciences) were used throughout the process for rapid aspiration and dispensing of molecular and cellular reagents. A Countess II image-based cell counter (Life Technologies) was used for measuring human cell population densities.

**Small-molecule chemical induction.** 1,000× stock small-molecule abscisic acid (100 mM, Sigma Aldrich), doxycycline (200 µg/mL, Fisher Scientific), and 4-hydroxytamoxifen (1 mM, Sigma Aldrich) were dissolved in 100% ethanol and stored at recommended temperatures. For transient transfection induction experiments, 2 h after transfection, small molecules were mixed with mammalian cell medium such that the concentrations were 25×; then, proper volumes were dispensed into wells such that the final concentration was 1×.

**Maintenance and generation of stable Jurkat T lymphocytes through electroporation, piggyBac-mediated integration, eukaryotic selection, and doxycycline induction.** Wild-type Jurkat T-lymphocyte cells were kept

in a humidified incubator at 37 °C and 5% CO<sub>2</sub> and maintained in RPMI medium (Corning) with 5% heat-inactivated fetal bovine serum (HI-FBS, Life Technologies), 50 UI/mL penicillin, 50 µg/mL streptomycin (Corning), and 2 mM glutamine (Corning). Prior to electroporation, cells were changed with medium containing 10% HI-FBS and without antibiotics. On days of transfection, cells were checked to be within  $5-8 \times 10^5$  cells/mL and  $2 \times 10^7$  cells were spun down at 300g and resuspended in 300 µL medium per transfection. Cell solutions were mixed with 20 µg transposon vector and 4 µg of transposase (pCAG-SuperPBBase, pBW900). After 15 min of room temperature incubation, DNA/cell mixtures were transferred to a 4-mm electroporation cuvette and electroporated in a Harvard Apparatus BTX instrument using a single pulse 300 V square wave for 10 msec. Cells were then transferred to 10% HI-FBS medium without antibiotics and placed into the incubator. One to two days later, cells were spun down and resuspended in medium with 5% HI-FBS with antibiotic and antieukaryotic chemicals. Puromycin (Thermo Scientific) was used at a final concentration of 2 µg/mL and zeocin (Invivogen) at 400 µg/mL. Antieukaryotic selections were performed for at least 10 d before removing antieukaryotic compounds.

For the experiment in **Figure 2b**, the decoder recombinase reporter (pBW2293) was first integrated and selected with zeocin; then, recombinase expression vectors (hPGK-iCre, hPGK-FlpO, hPGK-FlpO-2A-iCre) were integrated and selected for with puromycin in duplicate ( $n = 2$ ). After final stable line generation, 300,000 Jurkat cells of each line were spun down and resuspended in doxycycline or ethanol-containing medium. Cells were maintained in respective media for a given amount of time (14 d in ethanol and then with or without doxycycline for 3 d in **Figure 2b**, square points in **Supplementary Fig. 11**) and then run for cytometric readings.

**Flow cytometry.** Two days after transfection and after trypsinization (0.05% Trypsin/0.53 mM EDTA, Corning) and resuspension, all HEK293FT cell populations were analyzed using a Becton Dickinson (BD) LSRFortessa SORP flow cytometer with high-throughput sampler, except for data in **Figure 5**, which were recorded on a BD LSRII. Time-course data were obtained through trypsinization and fixation of cells at particular time points (BD Cytofix) and kept at 4 °C until analyzed through flow cytometry. The LSRFortessa was equipped for or detection of EGFP (488 nm laser, 530/30 emission filter, 505 longpass dichroic mirror), tagBFP (405 nm laser, 450/50 emission filter), mCherry or mRuby2 (561 nm, 610/20 emission filter, 595 longpass dichroic mirror), iRFP-720 (637 nm laser, 730/45 emission filter, 685 longpass dichroic mirror), and LSS-mOrange (405 nm, 610/20 emission filter, 535 longpass dichroic mirror). The LSRII was similarly equipped for detection of EGFP, tagBFP, mCherry and mRuby2, but with additional channels for iRFP-720 (633 nm laser, 720/40 emission filter, 710 longpass dichroic mirror) and LSS-mOrange (405 nm, 590/35 emission filter, 505 longpass dichroic mirror). All Jurkat T-lymphocyte experiments were run using a Life Technologies Attune NXT 4-laser acoustic focusing flow cytometer. The Attune NXT was equipped for detection of EGFP (488 nm laser, 510/10 emission filter), tagBFP (405 nm laser, 440/50 emission filter), mRuby2 (561 nm, 585/16 emission filter), iRFP-720 (638 nm laser, 720/30 emission filter) and LSS-mOrange (405 nm, 603/48 emission filter).

A gate was applied on forward scatter (FSC-A) and side scatter (SSC-A) to remove debris from cell populations in FlowJo (Tree Star) (**Supplementary Fig. 26**). pCAG-tagBFP or pCAG-LSS-mOrange plasmids were used as HEK293FT transient transfection markers and were gated for by applying a gate on the top 0–0.1% wild-type cells in those channels. Figure plots represent at least 5,000 events in the transfected cell subset. Compensation was applied for four and five-color experiments (**Supplementary Figs. 27, 28, and 29**). No gates other than a viable cell FSC/SSC were applied for Jurkat T-lymphocyte stable line experiments. To demonstrate the digital ON/OFF behavior of the genetic circuits, main text plots have additionally been expressed as a percentage of cells in an ON state through application of gates in fluorescent protein channels. Gates were chosen per experiment in an arbitrarily defined manner, but applied uniformly for all samples in each experiment (**Supplementary Figs. 1, 6, 13, 15, 19, and 21**).

**Quantitative real-time PCR analysis.** RNA was extracted from HEK293FT cells using the Qiagen RNeasy Plus Mini kit. 500 ng of RNA was

reverse-transcribed into cDNA using qScript cDNA SuperMix 20 µL reaction kit (Quanta BioSciences). cDNA samples were diluted to 100 µL using diethyl pyrocarbonate (DEPC)-treated water. Next, 5 µL of diluted cDNA was amplified using primers (**Supplementary Table 11**) through the use of the LightCycler 480 SYBR Green I Master polymerase kit (Roche) and a LightCycler 480 Instrument II (Roche). Relative fold-changes were determined using the  $\Delta\Delta C_t$  method.

**Vector proximity computational analysis.** Each desired 2-input 2-output Boolean function corresponded to a truth table with four rows and two output columns. The two output columns in each desired Boolean function  $f$  were mapped to an 8-dimensional binary vector  $\mathbf{t}$ , which we call the truth table vector. The fluorescent reporter signals measured from each of the two outputs, for each of the four input conditions from every genetic circuit implementation, were also mapped to an 8-dimensional real vector  $\mathbf{s}$ , which we call the signal vector. An ‘ideal implementation’ of  $\mathbf{t}$  is a circuit whose signal vector satisfies the equation  $\mathbf{s} = c \cdot \mathbf{t}$ , for some positive real number  $c$ . We quantified the correctness of a genetic circuit implementing Boolean function  $f$  by computing the angle  $\theta$  between the vectors  $\mathbf{t}$  and  $\mathbf{s}$  using the formula

$$\theta = \cos^{-1}\left(\frac{x}{y}\right),$$

where

$$x = \sum_{i=1}^8 t_i \cdot \hat{s}_i, y = \sqrt{\sum_{i=1}^8 t_i^2} \cdot \sqrt{\sum_{i=1}^8 \hat{s}_i^2},$$

and  $t_i$  and  $s_i$  are the  $i$ -th components of the vectors  $\mathbf{t}$  and  $\mathbf{s}$ . In computing  $\theta$ , we capped the signal values  $s_i$  to a maximum of  $2 \times 10^4$  a.u., denoted by  $\hat{s}_i$  in the formulae above. The angular difference ranges from  $0^\circ$  (best) to  $90^\circ$  (worst). We quantified the strength of the signal vector by computing its dynamic range ( $\delta$ ) of a genetic circuit implementation as  $\delta = \max_{\{i:t_i=1\}}(s_i) - \max_{\{i:t_i=0\}}(s_i)$ . We computed the dynamic range separately for the two outputs of each circuit and omitted the computation for circuits where the magnitude differences were not defined. Consequently, we had to omit two circuits (always ON GFP/always OFF mCherry, and always ON GFP and mCherry) from the  $\delta$  computation and 16 GFP or mCherry outputs of circuits (but not both) from the  $\delta$  computation.

**Statistical methods.** All transient gene expression experiments involved transfection of DNA into  $n = 3$  separate cell cultures. Fluorescence intensities for each cell culture population was averaged and the s.e.m. was taken. Stable integrations were performed once or in duplicate as indicated.

**Data availability.** Data are available from the corresponding authors upon reasonable request. Plasmids and construction resources are available at <https://www.addgene.org/browse/article/25012/>.